Proceedings of Computational Engineering Conference JSCES
Vol. 28, 2023 May

Safely evaluation of indoor spaces through simulation of CO2 exhalation and ventilation

Rahul Bale [1) 2)] Chung-Gang Li [3)] Kazuhide Ito [4)] and Tsubokura Makoto [5) 6)]

[1)]Graduate School of System Informatics, Kobe University (Kobe, Japan.)
[2)]RIKEN Center for Computational Science (Kobe, Japan, E-mail: rahul.bale@riken.jp)
[3)]Department of Mechanical Engineering, National Chung Hsing Univeristy (Taiwan. , E-mail: cgli@gs.ncku.edu.tw)
[4)]Faculty of Engineering Sciences, Kyushu University (Fukuoka, Japan. , E-mail: ito@kyudai.jp)
[5)]RIKEN Center for Computational Science (Kobe, Japan.)
[6)]Graduate School of System Informatics, Kobe University (Kobe, Japan. , E-mail: mtsubo@riken.jp)

The importance of indoor space safety has been highlighted due to the COVID-19 pandemic. Assessing indoor environments' safety by directly measuring human-generated air pollutants like CO2 has been suggested as one of methods to analyze indoor safelty. This is assuming a strong correlation between CO2 levels and the presence of infectious pathogens. This study examines the accuracy of this assumption by conducting a comparative analysis of infection risks in indoor settings using CO2 dispersion simulations and discrete droplet dispersion simulations.

Key Words : *COVID, Indoor Air contamination, Pathogen transmission*

1. INTRODUCTION

Airborne spread of virus-containing sputum droplets can lead to airborne disease transmission, posing a significant threat to public health. In recent decades, various highly infectious and communicable diseases have emerged, such as Severe Acute Respiratory Syndrome (SARS), H1N1 influenza, and Coronavirus Disease 2019 (COVID-19). Since its appearance, COVID-19 has quickly become a lethal pandemic, causing hundreds of millions of infections and millions of deaths (source: JHU COVID-19 resource). Moreover, the indirect impact of the pandemic due to job loss and major economic contraction is hard to measure. The evidence on COVID-19 so far indicates that potential modes of SARS-CoV-2 transmission include respiratory droplets, direct person-to-person contact, and contact with surfaces (fomite mode of transmission). Direct person-to-person transmission and fomite transmission can be reduced through proper hygiene practices, but controlling airborne transmission is much more difficult. As a result, airborne transmission is probably the main reason for COVID-19 becoming a global pandemic (Center for Disease Control, CDC, USA). The use of masks has been widely recognized and adopted as an effective way to limit airborne transmission. The importance of indoor ventilation and air circulation in reducing airborne transmission cannot be emphasized enough. A well-mixed indoor environment with a high air exchange rate per person can significantly improve indoor space safety. In light of this, a practical method for evaluating an indoor space's ventilation system is by measuring the CO_2 level within the space. This makes it easier for policymakers to issue guidelines for CO_2 levels in public indoor spaces. While measuring CO_2 levels and providing guidelines for them is convenient, it is uncertain whether the infection risk in indoor spaces due to airborne pathogens is strongly correlated with CO_2 levels. To this end, in this work, we conduct a comparative study to examine the correlation between CO_2 levels and infection risk in a simplified indoor space. We use infection risk assessment based on discrete droplet simulations as the foundation for the comparative analysis. We employ a fully compressible Navier-Stokes solver, where the evaporated phase of the droplet and its effect on droplet evaporation are modeled. A discrete Lagrangian droplet model is used to model droplet transport and evaporation. The droplet model is connected to the flow equations to enable weak two-way coupling between the droplets and the flow, where the droplets are affected by the flow, while the opposite is not allowed; however, the vapor phase of the droplets is influenced by droplet evaporation. CO_2 is modeled as a passive scalar through a species transport equation.

2. GOVERNING EQUATIONS

The sputum droplet dispersion is modelled through a combination of a Lagrangian frame for the droplet dynamics and the air/gas flow dynamics are modelled on a conventional fixed Eulerian mesh. The conservation equations for mass, momentum, energy are solved on the Eulerian mesh. Species transport equations are considered to account for the humidity variation around the mouth during a cough. The conser-

vation equations in the compact form are given by

$$\frac{\partial \mathrm{U}}{\partial t} + \nabla \cdot \mathbf{F} = \mathbf{S}, \tag{1}$$

where U and $\mathbf{F}$ are given below.

$$\mathrm{U} = \begin{pmatrix} [1.25]\rho \\ \rho u_1 \\ \rho u_2 \\ \rho u_3 \\ \rho e \\ \rho Y_k \end{pmatrix}, F_i = \begin{pmatrix} [1.25]\rho u_i \\ \rho u_i u_1 + P\delta_{i1} - \mu A_{i1} \\ \rho u_i u_2 + P\delta_{i2} - \mu A_{i2} \\ \rho u_i u_3 + P\delta_{i3} - \mu A_{i3} \\ \rho(\rho e + P)u_i - \mu A_{ij}u_j + q_i \\ \rho u_i Y_k - \rho \hat{u}_i^k Y_k \end{pmatrix},$$

$$\mathbf{S} = \begin{pmatrix} 0 \\ (\rho - \rho_0)g_1 \\ (\rho - \rho_0)g_2 \\ (\rho - \rho_0)g_3 \\ (\rho - \rho_0)g_i u_i \\ S_{\rho Y_k} \end{pmatrix}. \tag{2}$$

Here, the density of the gas/air is represented by ρ and the viscosity is given by μ. $\mathbf{u}$, e and P represent the velocity, total specific energy and the pressure, respectively. Species mass fraction and diffusion velocities of the k^{th} species are given by Y_k and $\hat{u}_i^k$, respectively. (u_1, u_2, u_3) are the components of the velocity vector $\mathbf{u}$ along the principal directions $1, 2, 3$. $\mathbf{g}$ is the acceleration due to gravity (eg. $\mathbf{g} = (0, 0, -9.81)m/s^2$). Of the species source terms $S_{\rho Y_k}$, the non-droplet vapor species are zero. The definition of the total specific energy is given by the following equation

$$e = \frac{P}{\gamma - 1} + \frac{1}{2}u_i u_i, \tag{3}$$

where γ is the ratio of the gas specific heat capacities. The heat flux $\mathbf{q}$ is given by

$$\mathbf{q} = -\lambda \nabla T, \tag{4}$$

where λ is the thermal diffusivity, and $\mathbf{A}$ is the velocity gradient tensor. The diffusion velocities of the chemical species may be expressed as a function of species diffusivity D_k as

$$\hat{\mathbf{u}}^k Y_k = D_k \nabla Y_k. \tag{5}$$

(1) Droplet Model

We adopt a one-way coupling approach for the droplet transport and evaporation model, wherein it is assumed that the effect of droplet motion and evaporation on the ambient air is negligible while the droplet transport and evaporation are directly linked to the airflow and temperature [3]. The equations modelling the transport, evaporation and the rate

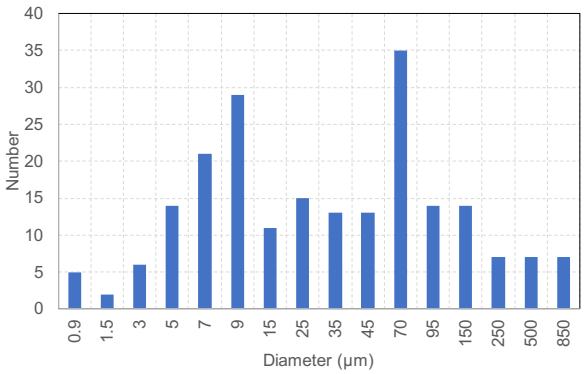

Fig. 1 a) Distribution of droplet diameter at the time of injection[1].

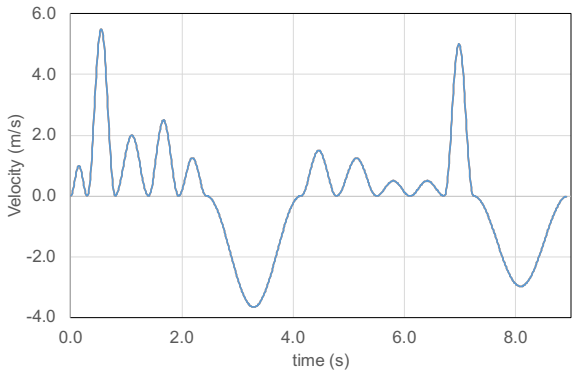

Fig. 2 The velocity profile of flow generated during the speech as function of time[2].

of change of droplet temperature are given by the equations below

Given below are the equations governing the rate of change of droplet mass, m_d, velocity, $\mathbf{u}_d$, temperature, T_d and position.

$$\frac{d\mathbf{x}_d}{dt} = \mathbf{u}_d, \tag{6}$$

$$\frac{d\mathbf{u}_d}{dt} = \frac{3C_D}{4d_d}\frac{\rho}{\rho_d}(\mathbf{u} - \mathbf{u}_d)|\mathbf{u} - \mathbf{u}_d|, \tag{7}$$

$$\frac{dT_d}{dt} = \frac{Nu}{3Pr}\frac{c_p}{c_l}\frac{f_1}{\tau_d}(T - T_d) + \frac{1}{m_d}\left(\frac{dm_d}{dt}\right)\frac{L_V}{c_{p,d}}, \tag{8}$$

$$\frac{dm_d}{dt} = -\frac{m_d}{\tau_d}\left(\frac{Sh}{3Sc}\right)\ln(1 + B_M). \tag{9}$$

Here, $\mathbf{x}_d$, $\mathbf{u}_d$, m_d, and T_d are the droplet position, velocity, mass and temperature, respectively. T is the temperature of the ambient air, L_v the latent heat of evaporation at the droplet temperature. c_p and c_l are the specific heat at constant pressure of the ambient air and the specific heat capacity of the liquid droplet, and τ_d is the response time of the droplet. f_1 is a correction to the heat transfer due to evaporation of the droplet[4]. Nu & Pr are the Nusselt and Prandtl

Table 1 The initial and flow conditions of the indoor setup.

Ventilation Flow rate (m^3/hr)	576
No. Air Exchanges (1/hr)	12
Inlet/Outlet Velocity (m/s)	1.778
Inlet CO_2 level (ppm)	400
Inlet Temp. (K)	300
AC Flow rate (m^3/hr)	1200
AC inlet velocity (m/s)	2.2371
AC inlet Temp. (K)	293
AC suction velocity (m/s)	0.7994
Room Temp. (K)	297
Ambient humidity (RH)	60
Human body surface Temp. (K)	300
Human exhalation CO_2 (ppm)	40000

numbers, respectively [5,6]. B_m is the mass transfer number (details of which can be found in [3]), and Sh & Sc are the Sherwood and Schmidt numbers, respectively. Under a unit Lewis number assumption $Pr = Sc$. For the evaluation of the Prandtl number the standard definition is used, where as the Nusselt number [7,8] is evaluated using the expression is given below along with the definition of τ_d.

$$\tau_d = \frac{\rho_d d_d^2}{18\mu} \tag{10}$$

$$Nu = 2 + 0.552 Re_s^{1/2} Pr^{1/3} \tag{11}$$

$$Sh = 2 + 0.552 Re_s^{1/2} Sc^{1/3} \tag{12}$$

In the above equation ρ_d is the density of the droplet and Re_s is the Reynolds number based on the slip velocity of a droplet with respect to the gas phase flow velocity, $\mathrm{u_{slip}} = \max(|\mathbf{u} - \mathbf{u_d}|)$

$$Re_s = \frac{\rho \mathrm{u_{slip}} \mathrm{d_d}}{\mu}. \tag{13}$$

The drag coefficient of the droplet, C_D, depends on its Reynolds number and is given by

$$C_D = \begin{cases} \frac{24}{Re_d}\left(1 + 1/6 Re_d^{2/3}\right) & Re_d < 1000, \\ 0.424 & Re_d > 1000, \end{cases} \tag{14}$$

and the droplet Reynolds number is given by

$$Re_d = \frac{\rho(\mathbf{u} - \mathbf{u}_d) d_d}{\mu}. \tag{15}$$

3. Simulation Setup

The mouth flow generated while counting from 1 to 10 in English is employed to model speech flow. The flowrate of speech is represented by $\dot{q} = A_i \sin^2(\pi t / T_i)$, where A_i and T_i denote the amplitude and period of the i^{th} utterance, respectively. To precisely model respiratory flow during speech, we include inhalation along with the expiratory flow of speech, ensuring mass balance of respiratory flow throughout one speech cycle. Inhalation phases are added after the words 'five' and '10', resulting in a net flow rate of one speech cycle equaling 0. The flow velocity when applying this speech model to a mouth opening with an area of 6 cm^2 is depicted in Fig. 2. The net flow rate of the speaking model is 22.74 L/min (or 3.388 L/cycle). While literature provides data on the size/area of mouth opening during a cough[9], information for speech is unavailable. Gupta et al.[9] report an average mouth opening area of 4 cm^2 for coughing. We assume that the mouth opening area for speech is slightly larger than that during a cough, choosing a value of 6 cm^2.

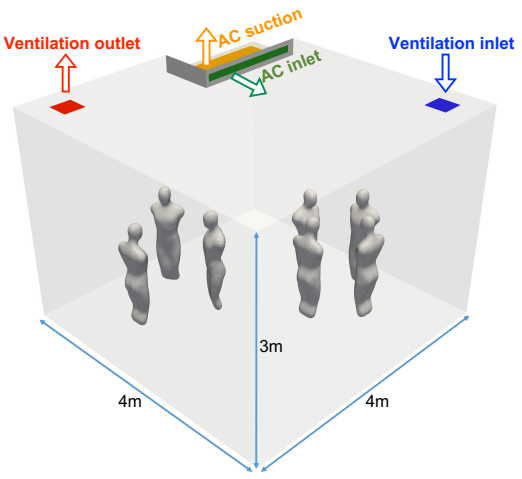

Fig. 3 The geometry of the indoor environment adopted for the present work along with the human subjects within the room.

Droplet size distribution reported in literature varies significantly. Loudon and Roberts, and Duguid and Chao et al. report peak droplet counts of 6 μm and 12 μm, respectively, while Xie et al.[10] report a value as high as 50 μm. Given the disparate droplet size distribution data in the literature, we adopt a combination of these figures. The droplet diameter distribution used in this work is illustrated in Fig. 2.. Droplets are injected into the domain at the circular mouth model at time instants corresponding to the peak velocity of each utterance.

The indoor space geometry utilized in this work is depicted in Fig.3. The room has a floor area of $4 \times 4 m^2$ and a height of 3 m. The ventilation system includes a fresh air inlet and a stale air outlet located on diagonally opposite roof corners. The room also features an air-conditioning system with a suction vent that removes air from the room and an inlet vent that supplies cool or hot air. Seven human subjects are represented by simplified human figurines in the room. The subjects are divided into two groups of three and four

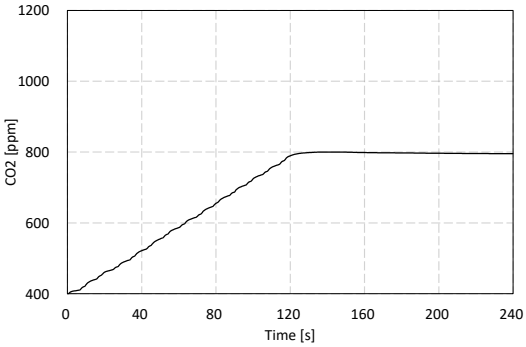

Fig. 4 Evolution of room averaged CO_2 level as the speaking model is turned off after 120s.

individuals facing each other, assuming conversation. During the simulation, all subjects are presumed to be speaking using the speech model shown in Fig.2. The ventilation rate, AC settings, and initial conditions are summarized in Table 1. A Neumann or zero gradient boundary condition is applied to scalar species such as H_2) and CO_2 at room outlet vents (Ventilation outlet and AC suction) and the mouth geometry during the inhalation phase. Finally, the net mass flux of all scalar species removed from the room through the AC suction vent is reintroduced via the AC inlet vent, assuming no mass loss and maintaining net scalar mass conservation

4. RESULTS

(1) Verification

The following verification case was adopted to confirm that the Dirichlet and Neumann boundary conditions used for scalar species are suitable and that the scalar species mass is conserved when recycled through the AC system. The ventilation system is deactivated, the AC system remains operational during the simulation, and the human subject's speaking model is switched off after 120s. This configuration aims to raise the CO_2 scalar mass in the room due to expiration during speech and maintain a stable value once the speaking model is turned off. The room's average CO2 mass, expressed in parts per million, is illustrated in Fig. 4. As intended by the setup, the CO_2 level in the room increases steadily until the speaking model is turned off at 120s, after which it remains constant. The simulation continues until 240s, during which the total mass of CO_2 scalar decreases by 0.5%.

(2) Comparison of aerosol and CO_2 distribution

Two distinct simulations were conducted to compare CO_2 levels and distribution with droplet/aerosol concentration and distribution: First, a scalar diffusion simulation was used to model CO_2 diffusion and accumulation within the indoor space. Second, a droplet dispersion simulation was performed to examine the dispersion dynamics of discrete droplets exhaled during speech. In both simulations, the simulation was run for 100s initially to develop the flow, followed by the exhalation of CO_2 and droplets. After starting CO_2 exhalation, the simulation continued for 900s, whereas the droplet dispersion simulation lasted for only 100s. The shorter duration of the droplet simulation is mainly due to the computational load imbalance resulting from droplet ac-

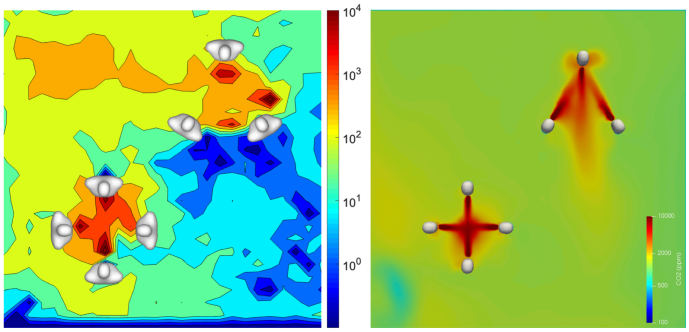

Fig. 5 A comparison of distribution of (left) virion concentration evaluated from droplet dispersion simulation and (right) CO_2 level minus the ambient CO_2 level (400ppm) on a plane located at 1.6m from the ground .

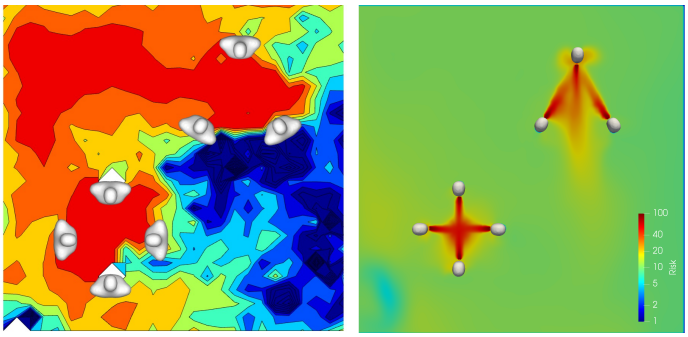

Fig. 6 The distribution of CO_2 and virion concentration in Fig. 5 converted to probability of infection.

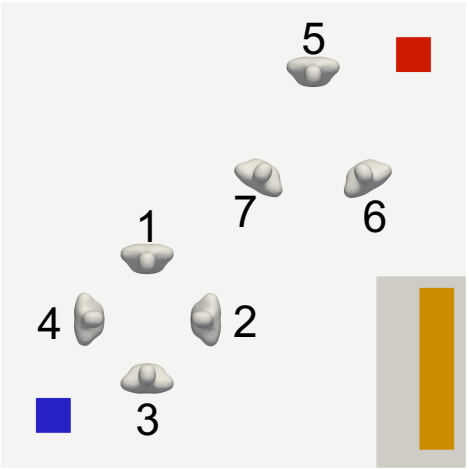

Fig. 7 Numbering of the human subjects

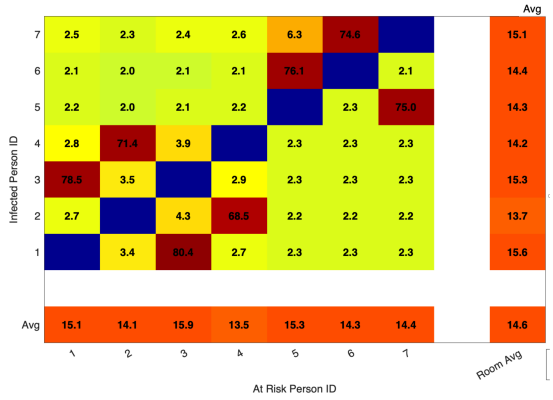

Fig. 8 The infection risk matrix for an exposure period of 15 mins based on CO_2 distribution. The color scheme of the matrix is matched with that of Fig. 9.

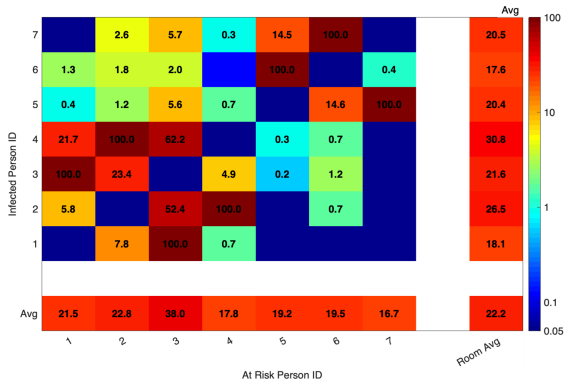

Fig. 9 The infection risk matrix for an exposure period of 15 mins based on the droplet distribution.

cumulation in certain areas of the computational domain. Nonetheless, we believe the comparison presented in this work will be informative and valuable to the reader.

The time-averaged distribution of CO_2 levels and virion concentration on a plane parallel to and situated 1.6m above the ground is shown in Fig.5. The droplet concentration on the mentioned plane can be converted into virion concentration by considering the virion density in the sputum. For further information on the conversion methodology and relevant parameters, readers are directed to our previous work [11]. The comparison demonstrates that the local distribution of droplets/virions and CO_2 differ significantly. This disparity becomes even more pronounced when the CO_2 and droplet distribution are converted into a probability of infection (the methodology details can be found in [11]), which is displayed in Fig.6. In both comparisons, the distribution between the human subjects is similar, with the primary difference arising in the area below the AC. In other regions, the difference is not as substantial.

(3) Comparison of person to person infection

The source contamination from human subjects can be separately tracked to assess the infection risk they pose to one another. To accomplish this, droplets emitted from each subject are marked with a unique identifier, and a distinct scalar transport equation is assigned to each subject to differentiate the CO_2 emitted by them. The number of human subjects is displayed in Fig.7. The person-to-person risk of infection can be evaluated using an infection risk matrix. The infection risk matrix based on CO_2 levels and droplet concentration under each subject's nose is presented in Figs.8&9. The infection matrix interpretation is as follows: the matrix rows represent an infected person, and the matrix columns represent a subject who may be at risk of becoming infected. The rows are numbered from bottom to top, the columns from left to right, and the numbers correspond to the person ID in Fig 7. The matrix entry corresponding to the first row and second column indicates the risk of infection for person 2 due to contaminants generated by person 1. The row labeled 'Avg' provides the average infection risk for a given person, considering contaminants from all other individuals in the room. Similarly, the 'Avg' column shows the average infection a given person is likely to cause due to contaminants generated by that person. Lastly, the matrix's bottom-right corner entry offers the room-averaged infection risk, assuming any one of the occupants may be randomly infected. Note that the matrix diagonal entries are, by definition, 0, as infected persons cannot infect themselves.

A comparison of the risk matrix reveals two main observations. First, the infection risk distribution within the matrix, the infection risk across the two groups, varies between the two methods. Second, the room and averaged infection risks are similar across the two methods, though not identical. Due to a more uniform distribution of CO_2 within the space, the infection risk of a subject from one group caused by an infected subject from the other group is non-zero and uniform. In contrast, the droplet simulation results indicate that individuals in groups 5-7 are less likely to be infected by persons in the 1-4 group, while persons in the 1-4 group are at risk due to individuals in the 5-7 group. This difference may result from the shorter simulation period of the droplet simulation. The person and room average infection risk are similar across the two methods mainly because the averaged data is dominated by a given subject's high infection risk due to a nearby neighbor.

5. Summary

This study offers a comparative examination of CO_2 diffusion and droplet dispersion simulations, with the main objective being to ascertain if CO_2 can serve as a suitable proxy for infection risk due to droplet inhalation in indoor environments. To achieve this, droplet dispersion simulation results, in terms of droplet and virion concentrations, were juxtaposed with CO_2 diffusion simulation outcomes. Our analysis revealed that the distribution of virion concentrations and

CO_2 levels within the indoor space varied. The disparity between the findings might stem from the droplet simulation duration being insufficient for yielding accurate steady-state statistics. Consequently, enabling a longer simulation duration for the droplet simulation is essential for a more dependable comparison. The person-to-person infection risk comparison exhibited greater consistency between the two methodologies since this approach primarily concentrates on the area between human subjects, where the agreement between the two methods is stronger.

REFERENCES

[1] J. Wei and Y. Li, "Airborne spread of infectious agents in the indoor environment," *American journal of infection control*, vol. 44, no. 9, pp. S102–S108, 2016.

[2] J. K. Gupta, C.-H. Lin, and Q. Chen, "Characterizing exhaled airflow from breathing and talking," *Indoor air*, vol. 20, no. 1, pp. 31–39, 2010.

[3] T. Kitano, J. Nishio, R. Kurose, and S. Komori, "Effects of ambient pressure, gas temperature and combustion reaction on droplet evaporation," *Combustion and Flame*, vol. 161, no. 2, pp. 551–564, 2014.

[4] M. Nakamura, D. Nishioka, J. Hayashi, and F. Akamatsu, "Soot formation, spray characteristics, and structure of jet spray flames under high pressure," *Combustion and Flame*, vol. 158, no. 8, pp. 1615–1623, 2011.

[5] M. Nakamura, F. Akamatsu, R. Kurose, and M. Katsuki, "Combustion mechanism of liquid fuel spray in a gaseous flame," *Physics of Fluids*, vol. 17, no. 12, p. 123301, 2005.

[6] Y. Baba and R. Kurose, "Analysis and flamelet modelling for spray combustion," *Journal of Fluid Mechanics*, vol. 612, pp. 45–79, 2008.

[7] W. Ranz and W. R. Marshall, "Evaporation from drops i," *Chem. eng. prog*, vol. 48, no. 3, pp. 141–146, 1952.

[8] W. Ranz and W. R. Marshall, "Evaporation from drops ii," *Chem. eng. prog*, vol. 48, no. 3, pp. 173–180, 1952.

[9] J. Gupta, C.-H. Lin, and Q. Chen, "Flow dynamics and characterization of a cough," *Indoor air*, vol. 19, no. 6, pp. 517–525, 2009.

[10] X. Xie, Y. Li, H. Sun, and L. Liu, "Exhaled droplets due to talking and coughing," *Journal of the Royal Society Interface*, vol. 6, no. suppl_6, pp. S703–S714, 2009.

[11] R. Bale, A. Iida, M. Yamakawa, C. Li, and M. Tsubokura, "Quantifying the covid19 infection risk due to droplet/aerosol inhalation," *Scientific reports*, vol. 12, no. 1, pp. 1–15, 2022.